Accelerator mass spectrometry measurement of the reaction ^{35}Cl$(n,\gamma)^{36}$Cl at keV energies

Stefan Pavetich,[1,2,3,4,*] Anton Wallner,[2] Martin Martschini,[1] Shavkat Akhmadaliev,[3] Iris Dillmann,[5,6,7] Keith Fifield,[2] Shlomi Halfon,[8] Tanja Heftrich,[9] Franz Käppeler,[10] Claudia Lederer-Woods,[11] Silke Merchel,[4] Michael Paul,[12] René Reifarth,[9] Georg Rugel,[4] Peter Steier,[1] Moshe Tessler,[12] Stephen Tims,[2] Mario Weigand,[9] and Leo Weissman[8]

[1]*VERA Laboratory, University of Vienna, 1090 Vienna, Austria*
[2]*Department of Nuclear Physics, Research School of Physics and Engineering, The Australian National University, 2601 Canberra, Australia*
[3]*Institute of Ion Beam Physics and Materials Research, Helmholtz-Zentrum Dresden-Rossendorf, 01328 Dresden, Germany*
[4]*Helmholtz Institute Freiberg for Resource Technology, Helmholtz-Zentrum Dresden-Rossendorf, 01328 Dresden, Germany*
[5]*TRIUMF, Vancouver, British Columbia, V6T 2A3, Canada*
[6]*Department of Physics and Astronomy, University of Victoria, Victoria, British Columbia V8W 2Y2, Canada*
[7]*Karlsruhe Institute of Technology (KIT), Campus North, Institute of Nuclear Physics, Karlsruhe, Germany*
[8]*Soreq NRC, 81800 Yavne, Israel*
[9]*Institute of Applied Physics, Goethe University Frankfurt, 60438 Frankfurt, Germany*
[10]*Karlsruhe Institute of Technology, Campus North, Institute of Nuclear Physics, 76131 Karlsruhe, Germany*
[11]*School of Physics and Astronomy, University of Edinburgh, Edinburgh EH9 3JZ, United Kingdom*
[12]*Racah Institute of Physics, Hebrew University, 91904 Jerusalem, Israel*

(Received 26 September 2018; published 8 January 2019)

The nuclide ^{35}Cl can act as a minor "neutron poison" in the stellar slow neutron capture process. Neutron activation combined with accelerator mass spectrometry (AMS) was applied to measure the (n,γ) cross section of ^{35}Cl for neutron spectra simulating Maxwell-Boltzmann distributions of $kT \approx 30$ and 40 keV. The neutron activations were performed at the Karlsruhe Van de Graaff accelerator and at the superconducting linear accelerator of the Soreq Applied Research Accelerator Facility utilizing the ^{7}Li$(p,n)^{7}$Be reaction. AMS measurements of the irradiated samples were performed at the 3 MV Vienna Environmental Research Accelerator, the 6 MV tandem accelerator at the Dresden AMS facility, and the 14 UD tandem accelerator of the Australian National University in Canberra. Our method is independent of previous measurements. For an energy of $kT = 30$ keV, we report a Maxwellian averaged cross section of 8.33(32) mb. Using this new value in stellar isotopic abundance calculations, minor changes for the abundances of ^{35}Cl, ^{36}Cl, and ^{36}S are derived.

DOI: 10.1103/PhysRevC.99.015801

I. INTRODUCTION

The slow neutron capture process (*s* process), consisting of series of neutron capture reactions and subsequent β^- decays, is one of the main stellar processes for the synthesis of heavy elements beyond iron [1,2]. The *s* process is driven by the neutrons produced in the reactions ^{13}C$(\alpha,n)^{16}$O and ^{22}Ne$(\alpha,n)^{25}$Mg. Lighter elements with high abundances and/or high neutron capture cross sections compete with the *s*-process nucleosynthesis of heavier elements by reducing the availability of neutrons. They can act either as "neutron absorbers," when the neutron is recycled in subsequent reaction steps [e.g., ^{16}O$(n,\gamma)^{17}$O$(\alpha,n)^{20}$Ne] or as "neutron poisons"' when the neutron is completely lost for the *s*-process nucleosynthesis [e.g., ^{14}N$(n,p)^{14}$C or ^{25}Mg$(n,\gamma)^{26}$Mg] [3]. Hence, these neutron poisons reduce the efficiency of the *s* process. Besides the most important neutron poisons ^{14}N and ^{25}Mg, there are several minor neutron poisons, including ^{35}Cl. Chlorine is the 17th most abundant element in the solar photosphere [4]. Apart from its role as a neutron poison, it is also prominently involved in the yet unsolved quest for the origin of ^{36}S [5,6].

Accurate knowledge of the capture cross section for neutrons with stellar energy distributions (Maxwellian averaged cross section, MACS) is necessary to determine the significance of ^{35}Cl and its impact on stellar reaction networks.

The existing measurements of ^{35}Cl(n,γ) cross sections at keV energies are based on the time-of-flight (TOF) method [7,8]. An independent method with different systematic uncertainties is important to resolve the existing discrepancies between experimental results on the one side and theoretical predictions but also results from nuclear database evaluations on the other side (see Sec. II). The high sensitivity of the activation method is beneficial as very thin samples can be used, making scattering corrections negligible. A second advantage of the activation method is that the direct radiative capture (DRC) component is included. The combination with accelerator mass spectrometry (AMS) [9–11] extends the activation method to cases where the reaction products have long half-lives (e.g., ^{36}Cl, $t_{1/2} = 3.013(15) \times 10^5$ yr [12]) and/or missing γ-ray transitions. Also uncertainties associated with

*Corresponding author: stefan.pavetich@anu.edu.au

TABLE I. Literature data for ^{35}Cl$(n,\gamma)^{36}$Cl for a MACS at 30 keV. All experimental data are based on measurements at ORELA.

Reference	$\bar{\sigma}_{\mathrm{MACS}}$ (30 keV) (mb)
Macklin (expt)[a] [7]	10.0(3)
Guber *et al.* (expt) [8]	9.39(29)
Woosley *et al.* (calc) [14][b]	11
NON-SMOKER (calc) [15][b]	15.9
MOST (2005) (calc) [16][b]	51.5
ENDF/B-VII.1 (eval) [17][c]	7.59
JEFF-3.2 (eval) [18][b]	7.54
JENDL-4.0 (eval) [19][b]	8.54
TENDL-2015 (eval) [20]	9.25
KADoNiS-1.0 (comp) [21][b]	9.39(29)

[a]expt = experimental data; calc = data from theoretical models; eval = evaluations of experimental data and theoretical models; comp = compilation.
[b]From http://exp-astro.physik.uni-frankfurt.de/kadonis1.0/
[c]Calculated, based on ENDF/B-VII.1 data.

branchings and isomeric states in the decay of the reaction product can be avoided by accelerator mass spectrometry.

II. PREVIOUS DATA

The first experimental determination of the MACS of ^{35}Cl was done by Macklin [7] by measuring the resonance parameters of 54 resonances between 4 and 220 keV. These measurements were performed at ORELA (Oak Ridge Electron Linear Accelerator) by bombarding a 3.91 mm thick LiCl target with a white neutron spectrum. A discussion of the systematic uncertainties of TOF measurements at ORELA is given in [13]. Further measurements at ORELA with reduced background from neutron scattering were performed by Guber *et al.* [8], providing data in the energy range between 0.0253 eV and 500 keV. The existing data base for ^{35}Cl(n,γ), relevant for stellar energies, is given in Table I as MACS for a stellar temperature equivalent to $kT = 30$ keV. The two experimental values are in reasonable agreement. For the recommended MACS of ^{35}Cl in KADoNiS (Karlsruhe Astrophysical Database of Nucleosynthesis in Stars) the most recent experimental value from Guber *et al.* [8] was adopted.

Statistical model calculations by Woosley *et al.* [14] and Rauscher and Thielemann [15] suggest 10%–70% higher values compared to the experimental data. The MACS calculated by the MOST code [16] is ≈5 times as high as the experimental data. Theoretical cross sections in this mass region can be uncertain because the used Hauser-Feshbach approach depends on a statistically significant ensemble of resonances, which is not guaranteed for light nuclei. However, according to [15] the NON-SMOKER model is applicable for ^{35}Cl and neutron energies above 26 keV.

Evaluated nuclear data libraries [17–20] predict somewhat lower values for the MACS (2%–30%) than the experimental data.

These discrepancies between experimental values, theoretical predictions and, evaluated data clearly emphasize the importance of a new measurement for the MACS of ^{35}Cl$(n,\gamma)^{36}$Cl by an independent method.

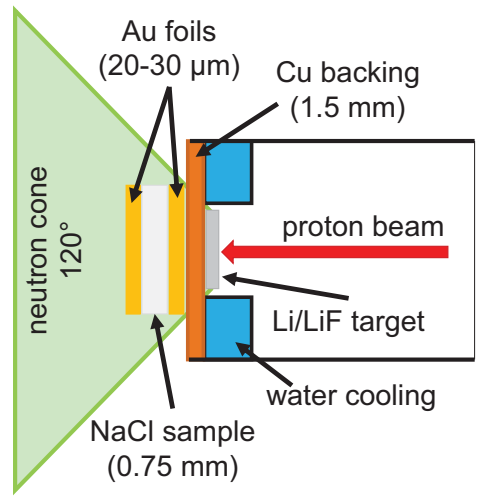

FIG. 1. Schematic of the activation setup at KIT.

III. EXPERIMENTAL METHODS

Neutron irradiations were performed at two facilities: the Van de Graaff accelerator of the Karlsruhe Institute of Technology (KIT) [22] and the Soreq Applied Research Accelerator Facility (SARAF) using the Liquid-Lithium Target (LiLiT) [23–25]. Subsequently, the ^{36}Cl/^{35}Cl isotope ratios of the irradiated samples were determined at the AMS facilities VERA (Vienna Environmental Research Accelerator) [26,27], DREAMS (DREsden AMS) [28–30], and HIAF (Heavy Ion Accelerator facility) [31] at the Australian National University.

A. Neutron activations

1. Activations at KIT

Commercial NaCl powder (Alfa Aesar 99.99% purity) of natural isotopic composition (^{35}Cl/^{37}Cl = 3.125(15) [32]) was pressed into two pellets, KIT1 and KIT2, each with a mass of 46.1 mg, a thickness of 0.75 mm, and a diameter of 6 mm. They were irradiated at the 3.7 MV Van de Graaff accelerator at KIT in separate beam times. A 30 μm thick Li target and a 30 μm thick LiF target, positioned on a water-cooled Cu plate, were used as primary targets for the irradiation of KIT1 and KIT2, respectively. The Li (LiF) target was bombarded with 1912 keV protons (see Fig. 1), 31 keV above the ^{7}Li$(p,n)^{7}$Be reaction threshold [33]. In this way, a neutron energy distribution is generated which almost perfectly resembles a 30 keV Maxwell-Boltzmann (MB) spectrum, but with a cutoff energy at 114 keV [22] (see Fig. 2). At the proton energy used, the neutrons are kinematically focused in a cone with an opening angle of 120°. The proton beam intensity for both irradiations was ≈100 μA and the beam was wobbled across the Li (LiF) samples to ensure a homogenous irradiation and thermal distribution of the beam over the target. The NaCl samples were positioned close to the

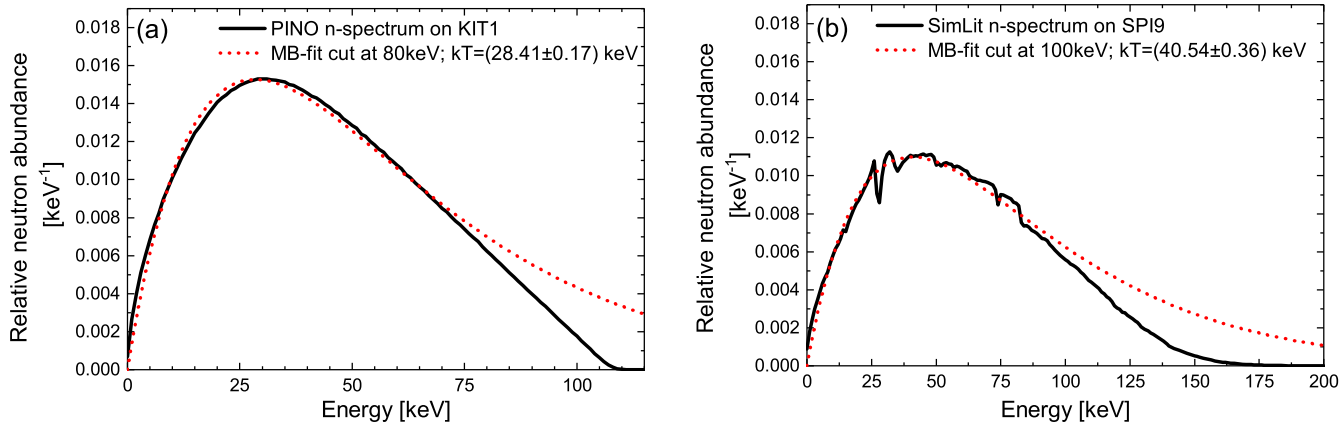

FIG. 2. Neutron irradiation spectra at KIT (a) and SARAF (b). The solid line shows the simulated neutron spectrum using the Monte Carlo codes PINO [35] (a) and SIMLIT [36] (b), respectively. The dashed-dotted lines show Maxwell-Boltzmann fits of the data cut at 80 and 100 keV, respectively, as the high-energy part of the distribution cannot be described by a MB fit.

neutron producing target (see Table II). The neutron emission cone covered the whole target. Gold foils, with thicknesses between 20 and 30 μm were attached to the front and back of the NaCl pellets as fluence monitors, utilizing the neutron induced ^{198}Au activity ($t_{1/2} = 2.6947(3)$ d [34]). A ^{6}Li-glass detector at 1 m distance from the neutron target was used to monitor relative changes in the neutron flux in intervals of 1 min. This monitoring was used to correct for changes in the neutron flux over time due to target degradation caused by the intense proton beam.

Sample KIT1 was irradiated in one session over ≈5 days (see Table II). The total neutron fluence was $1.16(6) \times 10^{15}$ cm^{-2}. Sample KIT2 was irradiated in a sandwich together with a Ni pellet and Au monitor foils in four consecutive activations. The total irradiation time for KIT2 was ≈10 days and the neutron fluence was $1.21(7) \times 10^{15}$ cm^{-2}. The LiF target and the Au foils were replaced between each activation session. In the first activation KIT2 and its back Au foil accidentally moved from their initial position at 2.7 mm distance to the LiF target to a distance of 3.1 mm. For this reason and due to additional inconsistencies in the neutron fluence (see Sec. IV A), the KIT2 data were not considered for the evaluation of the MACS.

The neutron energy distribution at the position of the target was simulated with the Monte Carlo tool PINO [35].

TABLE II. Parameters for the neutron activation at KIT and SARAF.

Sample	Distance to Li (mm)	Irradiation time (h)
KIT1	2.1	120.05
KIT2 total		249.12
KIT2a	3.1[a]	91.05
KIT2b	2.7	92.45
KIT2c	2.7	22.30
KIT2d	2.7	43.32
SPI9	6.0	2.0

[a]Accidentally moved from initial position of 2.7 mm (see text).

Figure 2(a) shows the simulated neutron energy distributions and MB distributions for 30 and 40 keV neutrons, respectively.

The activity of the Au foils was measured with a high-purity germanium (HPGe) detector of 2.12(4)% efficiency for the 411.8 keV ^{198}Au γ transition, which has an intensity of 95.62(6)% per decay [34].

2. Activations at SARAF

A third NaCl pellet was irradiated at the LiLiT beamline [23,24] at SARAF. For this activation a pellet (SPI9) pressed from Merck, CertiPUR® NaCl (purity >99.92%), with a mass of 203.9 mg, a thickness of 0.83 mm, and a diameter of 12 mm was used. The sample was sandwiched between Au foils of the same diameter and a thickness of ≈20 μm to determine the neutron fluence. This stack was mounted at 6 mm distance from LiLiT. Neutrons were generated via the ^{7}Li$(p,n)^{7}$Be reaction. LiLiT was specially developed to withstand the thermal load induced by proton beams with MeV energies and mA intensities [23,24]. This allows neutron production rates in the range of 10^{10}–10^{11} s^{-1}. The constant flow of liquid lithium reduces the aging (degenerative) effect of the proton beam on the target to negligible levels, in contrast to solid Li targets. The proton energy for the activation was 1930(3) keV, with an energy spread of ≈15 keV. The measurement of the proton beam parameters and their effect on the neutron spectrum are discussed in [37,38]. This lead to a neutron energy spectrum which resembled a Maxwell-Boltzmann distribution of ≈40 keV. The sample was irradiated for 2 h with an average proton current of 725 μA, resulting in a neutron fluence of $9.8(4) \times 10^{13}$ cm^{-2}. The proton current was measured by a modular parametric current transformer calibrated to a Faraday cup. Relative changes in the neutron flux were monitored with a fission chamber (6PFC16A, Centronic Ltd., UK), counting neutron-induced fission events from a 1 mg cm^{-2} thin internal uranium foil enriched in ^{235}U. This fission chamber was calibrated to a proton beam with a low intensity measured with a Faraday cup [24]. The resulting neutron spectra were simulated with

SIMLIT [36] and GEANT4 [39,40] for the positions of the Au foils and the NaCl samples. A coaxial HPGe detector (ORTEC GMX 25-83) at SARAF with an efficiency of 1.22(3)% for 411.8 keV was used for the Au-foil activity measurement.

B. Accelerator mass spectrometry

The number of ^{36}Cl atoms produced during the irradiations was determined by AMS. Typically, AMS determines isotopic ratios of long-lived radionuclides to stable nuclides (e.g., ^{36}Cl/^{35}Cl), by measuring count rates of the radioisotope with a particle detector and currents of the stable isotopes with Faraday cups. Reference samples (standards) with known isotopic ratios and blanks with no or negligible radioisotope content are used for normalization and background correction, respectively. The two samples activated at KIT were measured at the AMS facility VERA and the sample from SARAF was analyzed at DREAMS and HIAF.

The NaCl pellets were dissolved, homogenized, and converted into AgCl powder for the AMS measurements, following procedures slightly modified from [41,42] (see Appendix A1). This process also reduces the amount of sulfur hence also the content of ^{36}S, a stable isobar of ^{36}Cl.

The ^{36}Cl/^{35}Cl ratio was determined by the following procedure: AgCl samples with masses of ≈10 mg are loaded in the ion source. Cl^- ions are produced by bombarding the AgCl sample with Cs^+ ions. The negative ions are extracted from the ion source, pre-accelerated, and pass a first magnet. VERA and DREAMS also use an electrostatic analyzer for energy separation before the magnet. The ions of interest are injected into a tandem accelerator, where they are accelerated towards the positively charged terminal. Here, the injected particles pass a stripper foil or a gas stripper. In the interaction with the foil or the gas, electrons are stripped off from the negative ions. Molecules which passed the low-energy mass spectrometer and were injected into the accelerator are dissociated in the stripper. The resulting positive ions are accelerated towards the exit of the accelerator. A specific mass-over-charge ratio is selected by the analyzing magnet and an electrostatic filter. Isotopic (^{35}Cl, ^{37}Cl) and molecular background is reduced to negligible levels. The remaining background after this high-energy mass spectrometer is ^{36}S. The final particle identification and counting of the radionuclides is done with particle detectors. The stable isotopes ^{35}Cl and ^{37}Cl and the radioisotope ^{36}Cl are injected into the accelerator sequentially. Currents of ^{35}Cl and ^{37}Cl are measured and used to monitor the source output. Together with the ^{36}Cl count rate they provide the ^{36}Cl/Cl ratio.

1. AMS at VERA

For the AMS measurements at VERA [43–45] in total eight AMS samples from KIT1 and four AMS samples from KIT2 were prepared. In order to reduce interference from the isobar ^{36}S the AgCl powder was pressed onto AgBr backings, which are low in sulfur [27]. The ^{36}Cl/^{35}Cl ratios were determined during six AMS measurement series. In the data evaluation all values were normalized to the standard material SM-Cl-11 [^{36}Cl/^{35}Cl = 1.424(13) × 10^{-11}] [46] (for details see Appendix A2). Nonirradiated NaCl material (from the same supplier as the material for the KIT samples), which underwent the same chemical treatment as the KIT samples, was used as blank material at VERA. Terminal voltages between 3.0 and 3.3 MV were available and after foil stripping the 7+ charge state was selected for these measurements. This resulted in ion energies between 24.0 and 26.4 MeV. The isotopes of interest (^{35,36,37}Cl) were injected sequentially five times per second. A combination of a compact ionization chamber [47] and a silicon strip detector was used for the identification and counting of ^{36}Cl [26,27]. Currents of the stable ^{35}Cl and ^{37}Cl isotopes were measured with off-axis Faraday cups after the analyzing magnet. Activated, standard, and blank samples were repeatedly measured. The irradiated samples and the standard materials had ^{36}Cl/^{35}Cl isotopic ratios of ≈10^{-11}, well above the background ratios of 10^{-15}–10^{-14} measured for blank samples. More details on ^{36}Cl measurements at VERA can be found in Refs. [26,27].

2. AMS at DREAMS

Three AMS samples were produced from the irradiated material SPI9 for the measurements at DREAMS, where Cu target holders without any backing were used [29,48]. Additional NaCl powder (same material as SPI9) which underwent the same chemical pretreatment but was not irradiated (SPI2) was used as blank material for the AMS measurements at DREAMS and HIAF. The SPI9 samples and three blank samples, made from the SPI2 material, were measured relative to SM-Cl-11 [46]. Chemical sample preparation for all samples measured at DREAMS and at HIAF was performed at the DREAMS facility. Each of the AMS samples was measured at least three times for twenty minutes [28]. The DREAMS facility [28,30] is based on a 6 MV Tandetron accelerator. A bouncer system at the low-energy side switches between the three masses of interest with a frequency of 90 Hz, allowing quasi-simultaneous injection into the accelerator. The terminal voltage for the measurements was 5.886 MV. Argon was used as stripper gas and the 5+ charge state was chosen with the analyzing magnet. The $^{35,37}Cl^{5+}$ currents are measured in two offset Faraday cups downstream from the analyzing magnet. For additional suppression of ^{36}S a 1 μm thick silicon nitride foil and a subsequent 35° electrostatic analyzer (ESA) are used. The resulting sulfur suppression allows the usage of Cu cathodes without any backing in the first place. A four-anode ionization chamber is used for the final identification of ^{36}Cl [30].

3. AMS at HIAF

Four AMS samples of SPI9 were produced for the AMS measurement at HIAF [31,49]. Similar to VERA, at HIAF the AgCl samples are pressed onto an AgBr backing [49]. Three AMS samples produced from SPI9 and two samples of the SPI2 blank material were measured relative to the standard SM-Cl-11. A single measurement on a SPI9 sample was performed in a separate beam time. This measurement showed a significant deviation from the other measurements, was considered as outlier, and could be neglected for the further data evaluation due to its low weight (single measurement only). At HIAF a terminal voltage of 13.1 MV

was used. Argon stripping was used for the measurements and the 7+ charge state was selected by the analyzing magnet. The $^{35,37}Cl^{7+}$ currents are measured in a retractable inline Faraday cup in front of the detector. The radionuclide was counted with a five-anode ionization chamber. At HIAF slow sequencing was used for the measurement of the three Cl isotopes of interest: typically first the $^{35,37}Cl^{7+}$ currents are measured for ten seconds each, then ^{36}Cl is counted in the detector for 2–5 min. Then the currents are measured again. This sequence was repeated 2–3 times per sample. By scaling the terminal voltage between the ^{35,36,37}Cl beams appropriately the magnetic rigidity of the three isotopes is kept constant. The resulting larger difference of the velocities at the terminal leads to bigger differences in the charge state yields for the three isotopes.

IV. DATA ANALYSIS

The cross sections σ_{SACS} for the various irradiations were calculated from the respective total neutron fluence Φ_n (see Table IV):

$$\sigma_{\mathrm{SACS}} = \frac{^{36}\mathrm{Cl}}{^{35}\mathrm{Cl}} \frac{1}{\Phi_n}. \quad (1)$$

A. Neutron fluence

The neutron fluence during the irradiations was calculated from the number of produced ^{198}Au nuclei. With the corrections for the waiting time t_w (between the end of the irradiation and the beginning of the measurement), the measurement time t_m, and the γ -ray self-absorption, the number of produced ^{198}Au nuclei at the end of an irradiation is given by

$$N_{198} = \frac{C(t_m)}{\varepsilon I k (1 - e^{-\lambda_{\mathrm{Au}} t_m}) e^{-\lambda t_w}}. \quad (2)$$

Here, $C(t_m)$ is the number of ^{198}Au decays during the activity measurement, λ_{Au} is the decay constant of ^{198}Au, I is the relative intensity of the 411.8 keV ^{198}Au γ line, and ε is the detector efficiency. The self-absorption factor for the Au foils, k, was between 0.994 and 0.996. The number of produced ^{198}Au atoms is also given by

$$N_{198} = N_{197} \langle\sigma\rangle_{\mathrm{ENDF,S}}(^{197}\mathrm{Au}) \Phi_n f_b, \quad (3)$$

where N_{197} is the number of ^{197}Au atoms in the respective Au foil, $\langle\sigma\rangle_{\mathrm{ENDF,S}}(^{197}\mathrm{Au})$ is the spectrum averaged cross section for $^{197}\mathrm{Au}(n,\gamma)$, calculated by convolution of the ENDF/B-VII.1 energy-differential cross section data with the simulated neutron spectra. This spectrum averaged cross section is slightly different for different geometries and energy distributions, hence it differs between irradiations. Φ_n is the neutron fluence and

$$f_b = \frac{\int_0^{t_i} \phi(t) e^{-\lambda_{\mathrm{Au}}(t_i - t)} dt}{\int_0^{t_i} \phi(t) dt} \quad (4)$$

is a correction considering the decay of ^{198}Au during the irradiation time t_i and possible variations of the neutron flux $\phi(t)$. This factor can be calculated from the relative neutron flux data recorded with the ^{6}Li-glass detector (KIT) or the fission chamber (SARAF), respectively.

TABLE III. Correction factors f_b and neutron fluences at KIT and SARAF. The neutron fluence at the sample position is calculated as average of the fluences of the front and back Au foil. The last column gives the ratio of the neutron fluences calculated from the front and back Au foils.

Sample	f_b	Neutron fluence (10^{14} cm^{-2})			Ratio
		Au front	Au back	NaCl	front/back
KIT1	0.53	12.3(7)	10.8(6)	11.6(6)	1.14
KIT2 total				12.1(7)	
KIT2a	0.63	4.35(24)	3.85(21)	4.10(22)	1.13
KIT2b	0.63	4.90(27)	3.50(19)	4.20(23)	1.40
KIT2c	0.91	1.04(6)	0.72(4)	0.88(5)	1.44
KIT2d	0.79	3.36(18)	2.41(13)	2.88(16)	1.40
SPI9	0.986	1.03(4)	0.92(4)	0.98(4)	1.12

By combining Eqs. (2) and (3), the neutron fluence on the respective Au foils is

$$\Phi_n = \frac{C(t_m)}{\varepsilon I k f_b (1 - e^{-\lambda_{\mathrm{Au}} t_m}) e^{-\lambda t_w} N_{197} \langle\sigma\rangle_{\mathrm{ENDF,S}}(^{197}\mathrm{Au})}. \quad (5)$$

The neutron fluence on the NaCl sample was calculated as the average of the fluences obtained with the two gold foils. The respective neutron fluences at the positions of the Au foils, the neutron fluences at the NaCl sample position with their uncertainties (see Sec. IV C), as well as the f_b factors are listed in Table III. For KIT1, SPI9, and the first irradiation of KIT2 the ratio of the fluences calculated from the front and back foils is 1.12–1.14. In the other irradiations of KIT2 this ratio is ≈1.4. This inconsistency, together with the position shift during the first irradiation of KIT2 led to the decision to discard the KIT2 data.

B. Isotopic ratios

Examples of identification spectra from AMS measurements are plotted in Fig. 3. As these measurements were undertaken at three different facilities, the evaluation procedures differ in their details (see Appendix A2). Basically, the measured ratios were corrected for background and were all normalized to the same standard material, SM-Cl-11. Background corrections were negligible. Normalized ^{36}Cl/^{35}Cl ratios measured on the individual AMS samples, their weighted average, and the uncertainty of the average are plotted in Fig. 4. Note a small difference ($\leqslant$0.3%) between the plotted averages in Fig. 4, compared to the final averaged value in Table IV, due to a different averaging procedure to avoid correlation inaccuracies. The ^{36}Cl/^{35}Cl ratios of SPI9 measured at DREAMS seem to be slightly higher than the values measured at HIAF (see Fig. 4). Taking into account the uncertainty of the respective normalization factor (see Appendix A 2) the ^{36}Cl/^{35}Cl ratios of SPI9 measured at DREAMS and HIAF are in agreement.

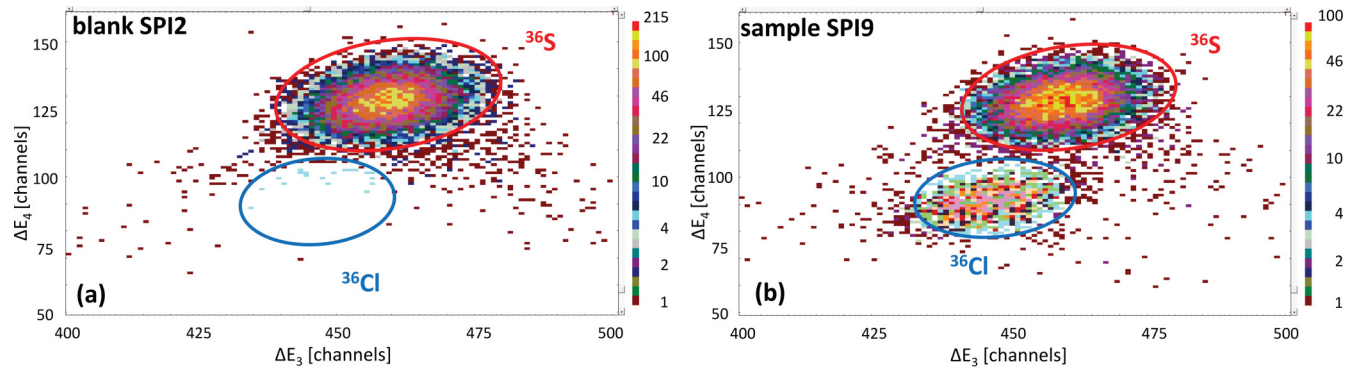

FIG. 3. Identification spectra for a blank (a) and the irradiated sample SPI9 (b) as obtained at DREAMS. As an example the energy-loss signal from the third anode (ΔE_3) is plotted versus the energy-loss signal from the fourth anode (ΔE_4). Additional energy-loss signals from the other two anodes were combined to improve the identification.

C. Uncertainty analysis

The individual uncertainty contributions are summarized in Table V.

For the KIT samples the dominating contributions are systematic uncertainties of the irradiation and the uncertainty of the efficiency of the HPGe detector. The standard deviation and the statistical uncertainty of the AMS measurement were very small, $\leqslant 0.5\%$ for KIT1 and KIT2 (see Fig. 4). Hence, their final AMS measurement uncertainty was derived from the typical reproducibility of AMS measurements of Cl at VERA (see Table V).

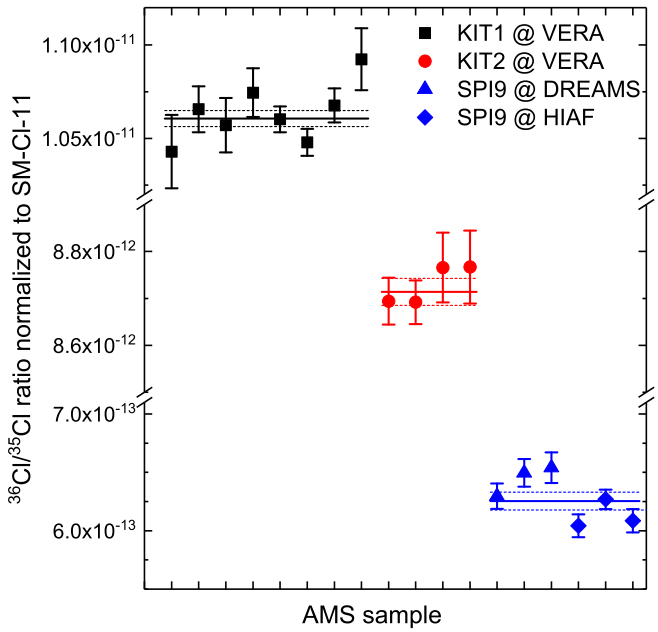

FIG. 4. ^{36}Cl/^{35}Cl ratios for the three neutron irradiated samples measured at the three AMS facilities with their uncertainties. The solid lines are the weighted averages of all individual AMS samples from the same material. The dashed lines show the associated uncertainties. Due to the inconsistencies during the neutron irradiation of KIT2 (see Sec. IV A), the KIT2 data was not considered for the calculation of the MACS.

For the SPI9 sample the dominating uncertainties are uncertainties associated with the shape of the neutron spectrum (simulation and positioning of the target) and the uncertainty of the HPGe detector efficiency. The uncertainty of the AMS measurement is more significant than for the KIT samples. It is determined from the typical reproducibilities for Cl AMS measurements at DREAMS and HIAF.

V. RESULTS

A. Maxwellian averaged cross section

In stellar environments neutrons are quickly thermalized by interactions with the stellar plasma, and thus the neutron energy distribution corresponds to a Maxwell-Boltzmann spectrum.

The neutron spectra produced via the ^{7}Li$(p,n)^7$Be reaction at KIT and SARAF closely reproduce Maxwell-Boltzmann neutron-energy distributions with $kT \approx 30$ keV and $kT \approx 40$ keV, respectively (see Fig. 2). The ratio of these measured cross sections and $\langle\sigma\rangle_{\mathrm{ENDF,S}}$, the cross section calculated from the resonance parameters in the ENDF/B-VII.1 database [17] averaged over the simulated neutron distribution is

$$f_c = \frac{\sigma_{\mathrm{SACS}}}{\langle\sigma\rangle_{\mathrm{ENDF,S}}}. \tag{6}$$

TABLE IV. Mean values for the irradiated samples and respective blank values at the individual AMS facilities.

Sample	^{36}Cl/^{35}Cl ratio (10^{-12})
KIT1 at VERA	10.60(7)
KIT2 at VERA	8.69(9)
SPI9 at DREAMS	0.643(12)
SPI9 at HIAF	0.617(19)
SPI9 average	0.627(13)
Blank at VERA	0.001–0.01
SPI2 blank at DREAMS	0.0014(5)
SPI2 blank at HIAF	0.00050(29)
SM-Cl-11 standard [46]	14.24(13)

TABLE V. Individual uncertainties of the activity and AMS measurements and the neutron spectra simulations.

Source of uncertainty	Uncertainty (%)		
	KIT1	KIT2	SPI9
Sample mass	1.0	1.0	0.5
γ ray intensity	0.06	0.06	0.06
Efficiency of HPGe detector	2.0	2.0	2.4
$\langle\sigma\rangle_{\mathrm{ENDF,S}}(^{197}\mathrm{Au})$	1.4	1.4	1.4
Neutron spectra	5.0	[a]	3.2
Positioning and stability of beam			2.5
Simulation of spectra			2.0
Statistics activation	0.16	0.11	0.23
Natural $\frac{^{35}\mathrm{Cl}}{^{37}\mathrm{Cl}}$ ratio	0.43	0.43	0.43
Nominal $\frac{^{36}\mathrm{Cl}}{^{35}\mathrm{Cl}}$ ratio of SM-Cl-11	0.94	0.94	0.94
AMS measurement uncertainty	0.71	1.00	2.13

[a]Unknown due to position shift during first irradiation (see Sec. III A 1).

The spectrum averaged value $\langle\sigma\rangle_{\mathrm{ENDF,S}}$ was calculated by

$$\langle\sigma\rangle_{\mathrm{ENDF,S}} = \frac{\sum_{E_{\min}}^{E_{\max}} \sigma(E_n)\varphi(E_n)\Delta E_n}{\sum_{E_{\min}}^{E_{\max}} \varphi(E_n)\Delta E_n}. \quad (7)$$

Here, ΔE_n is the energy interval and $\varphi(E_n)$ gives the relative number of neutrons per unit of energy in the according energy interval of the experimental neutron spectrum. The simulated neutron spectra were cut off at 114 and 200 keV in the PINO and SIMLIT simulations, respectively. The relative number of neutrons becomes negligible beyond these energies.

The calculation of the ratio f_c was done individually for both samples.

A weighted average ratio $\bar{f}_c$ of the two individual values (KIT1, SPI9) was determined. The uncertainties of the two individual values were used as weights. Using this weighted mean value $\bar{f}_c$ the Maxwellian averaged cross section for $^{35}\mathrm{Cl}(n,\gamma)^{36}\mathrm{Cl}$ at $kT = 30$ keV is given by

$$\bar{\sigma}_{\mathrm{MACS}} = \frac{2}{\sqrt{\pi}} \bar{f}_c \langle\sigma\rangle_{\mathrm{ENDF,MB}}, \quad (8)$$

where $\frac{2}{\sqrt{\pi}}$ is a normalization factor [22] and

$$\langle\sigma\rangle_{\mathrm{ENDF,MB}} = \frac{\sum_{E_{\min}}^{E_{\max}} \sigma(E_n) E_n e^{-\frac{E_n}{kT}} \Delta E_n}{\sum_{E_{\min}}^{E_{\max}} E_n e^{-\frac{E_n}{kT}} \Delta E_n}, \quad (9)$$

where ΔE_n is the energy interval and $E_n e^{-\frac{E_n}{kT}}$ is proportional to the relative number of neutrons per eV in the corresponding energy interval for a 30 keV neutron Maxwell-Boltzmann distribution. The summation is from $E_{\min} = 0.01$ meV to $E_{\max} = 20$ MeV and corresponds to the range of the ENDF/B-VII.1 data. Using $\bar{f}_c$ from Eq. (6) is justified due to the close similarity between the neutron-energy distributions with a real Maxwell-Boltzmann spectrum and the simulated spectra. For the uncertainty of the MACS only the uncertainty of $\bar{f}_c$ was considered.

The MACS deduced from sample KIT1 was found to be 13% higher than the ENDF value. The MACS for SPI9 with an uncertainty of 4.5% was found to be 7% higher than the ENDF value. The combined value for $\bar{\sigma}_{\mathrm{MACS}}(30\ \mathrm{keV})$ is ≈10% higher than the ENDF value (see Table VI).

TABLE VI. Measured cross sections, correction factors f_c, and the weighted final MACS for 30 keV.

	KIT1	SPI9
σ_{SACS} (mb)	9.2(5)	6.42(29)
$\sigma_{\mathrm{ENDF,S}}$ (mb)	8.10	5.99
f_c	1.13(6)	1.07(5)
weighted $\bar{f}_c$		1.10(4)
$\bar{\sigma}_{\mathrm{MACS}}(30\ \mathrm{keV})$		8.33(32)

B. Comparison to previous values

To calculate the MACS for energies in the range $kT =$ (2–100) keV the cross section obtained from the ENDF/B-VII.1 data was scaled by $\bar{f}_c$. The results are summarized in Table VII. In Fig. 5 they are plotted together with data given by Macklin [7] and Guber *et al.* [8] and the cross sections obtained with the resonance parameters from the ENDF/B-VII.1 database [17].

In Fig. 6 the MACS at $kT = 30$ keV from this work is compared to previous data and theoretical predictions. Our value agrees with the value calculated from the JENDL-4.0 database [19], within 1σ uncertainty. It is higher than the value calculated from the ENDF data, but supports a smaller MACS value than the TOF measurements and theoretical results

TABLE VII. MACS for $^{35}\mathrm{Cl}(n,\gamma)^{36}\mathrm{Cl}$ calculated from the measured MACS and scaled with the energy dependency from the ENDF/B-VII.1 database. Our data are compared to MACS from Refs. [7,8] and to cross sections directly deduced from ENDF/B-VII.1 data [17].

kT	$\bar{\sigma}_{\mathrm{MACS}}$ (mb)			
(keV)	This work	Guber *et al.* [8]	Macklin [7]	ENDF [17]
2	40.2(15)	52.9(16)		36.70
5	23.1(9)	27.7(8)	26.0	21.08
8	21.0(8)	23.9(7)		19.17
10	19.3(7)	21.6(6)	22.3	17.58
15	15.1(6)	16.7(5)	17.6	13.77
20	12.0(5)	13.3(4)	14.1	10.95
23	10.62(4)	11.83(36)		9.68
25	9.85(38)	11.01(33)	11.7	8.98
30	8.33(32)	9.39(29)	10.0(3)	7.59
35	7.22(28)	8.22(25)		6.59
40	6.40(24)	7.34(23)	7.9	5.83
45	5.76(22)	6.66(22)		5.26
50	5.26(20)	6.13(21)	6.6	4.80
60	4.53(17)	5.36(20)	5.8	4.13
70	4.01(15)	4.83(20)		3.66
80	3.62(14)		4.8	3.31
85	3.46(13)	4.32(22)		3.16
90	3.32(13)			3.03
100	3.08(12)	3.99(25)	4.1	2.80

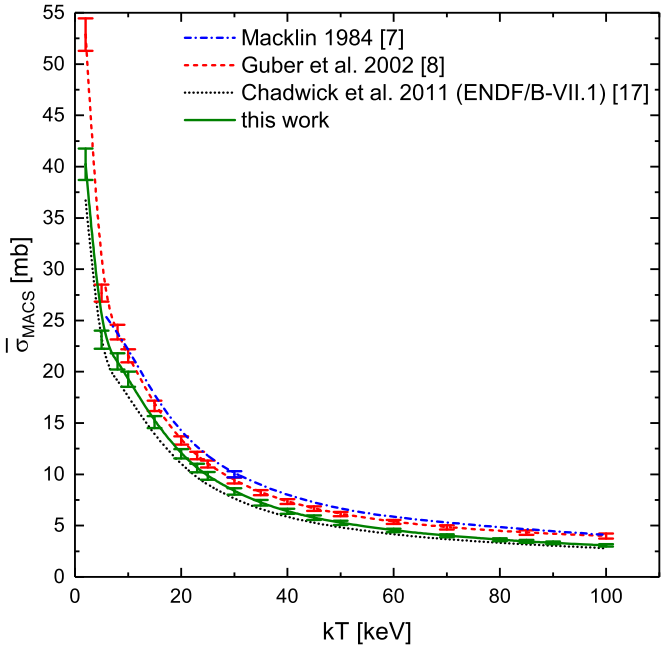

FIG. 5. MACS from this work for energies in the range $kT =$ (2–100) keV compared to the values of Macklin [7] and Guber *et al.* [8], and the results obtained directly with the resonance parameters from ENDF/B-VII.1 [17].

calculated with generic statistical model codes. The value for the MACS at 30 keV presented in this work follows the trend that a combination of activation and AMS measurements gives

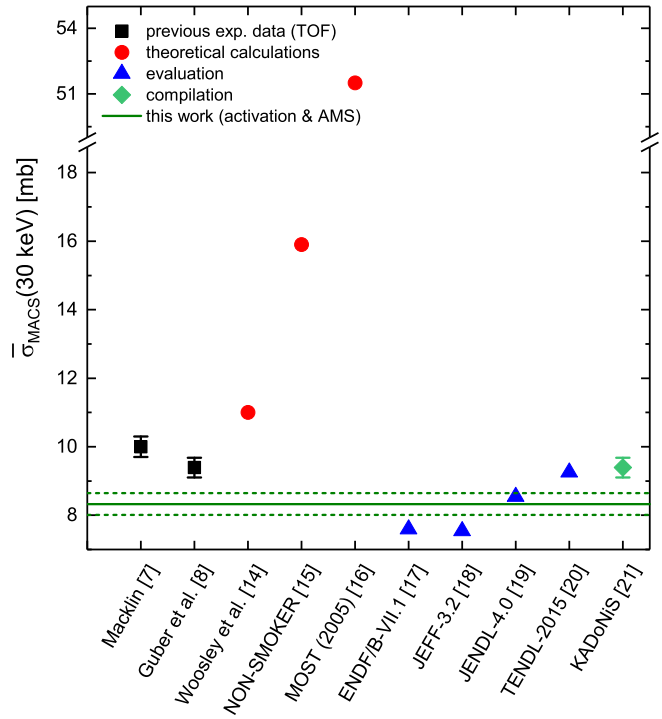

FIG. 6. MACS at $kT = 30$ keV from this work compared to previous values.

smaller values than previous TOF measurements (see, e.g., [50–53]).

C. Astrophysical implications

The effect of the new MACS of ^{35}Cl on the *s*-process abundance distribution has been investigated by means of the post-processing code NETZ [54,55]. Stellar models for the *s* process in thermally pulsing low-mass asymptotic giant branch (TP-AGB) stars and in massive stars, corresponding to the main and weak *s* components, respectively, have been studied as discussed in [55]. The calculations for both scenarios have been carried out using the standard set of MACS data from the KADoNiS compilation [21] and by replacing the MACS data of ^{35}Cl with the present results.

The comparison of the abundance distributions for both the main and weak components showed that the poisoning effect of ^{35}Cl was not altered by more than 0.1% by the new cross section. The only non-negligible abundance changes were found for ^{35}Cl itself, which increased by 10% in both TP-AGB and massive stars according to the smaller new MACS values. These changes had a minor influence on the abundance of ^{36}Cl and ^{36}S, which were both reduced by about 1 and 2% in TP-AGB stars and massive stars, respectively.

VI. CONCLUSIONS

The ^{35}Cl$(n,\gamma)^{36}$Cl cross sections for neutron spectra following quasi-Maxwell-Boltzmann distributions at $kT =$ 30 keV and 40 keV was measured and scaled to 30 keV, the classical energy for *s*-process nucleosynthesis [56]. The new result for the MACS at $kT = 30$ keV of 8.33(32) mb was deduced by an independent and complementary method using neutron activation and AMS. The value obtained in this work is 13%–20% lower than previous values obtained with the TOF method [7,8]. This new value leads to minor changes in the stellar abundances of ^{35}Cl, ^{36}Cl, and ^{36}S.

ACKNOWLEDGMENTS

Parts of this research were carried out at the Ion Beam Centre (IBC) at the Helmholtz-Zentrum Dresden-Rossendorf e. V., a member of the Helmholtz Association. C.L.-W. acknowledges support from the Science and Technology Facilities Council UK (ST/M006085/1) and the European Research Council ERC-2015-STG No. 677497>. I.D. is supported by the Canadian NSERC Discovery Grants No. SAPIN-2014-00028 and No. RGPAS 462257-2014.

APPENDIX A: ACCELERATOR MASS SPECTROMETRY

1. Sample preparation

The AMS sample preparation at VERA and DREAMS for the KIT and SARAF samples, respectively, was done following slightly modified procedures as described in Refs. [41,42]. The goals of the Cl sample preparation are to homogenize the sample material, bring it in a suitable form for the AMS

measurement (AgCl), and to reduce the sulfur content in the material. ^{36}S is a stable isobar to ^{36}Cl and it is orders of magnitude more abundant. Without chemical reduction the ^{36}S background would be too high for the AMS measurements.

The NaCl pellets were completely dissolved in deionized H_2O, or 1.4 M HNO_3, ensuring a homogenous mixture of the irradiated sample material. AgCl was precipitated by addition of $AgNO_3$ to several aliquots of the original solutions. The precipitate was centrifuged and the supernatant liquid discarded. The AgCl was redissolved in NH_3 and $Ba(NO_3)_2$ was added to trigger $BaSO_4$ coprecipitation with $BaCO_3$. The precipitate was removed by filtration [57]. HNO_3 was added to the solution and AgCl reprecipitated. The samples were centrifuged, decanted, washed with deionized water, and dried at 75–80 °C for several hours.

2. Data evaluation isotopic ratios

For the evaluation of the AMS data first the sulfur corrected isotopic ratios were calculated by

$$\frac{^{36}\mathrm{Cl}}{^{35}\mathrm{Cl}} = \frac{C_{^{36}\mathrm{Cl}} - f_\mathrm{S}\, C_{^{36}\mathrm{S}}}{I_{^{35}\mathrm{Cl}}\, t_{36}}\, e\, q, \tag{A1}$$

where $C_{^{36}\mathrm{Cl}}$ and $C_{^{36}\mathrm{S}}$ are the numbers of ^{36}Cl and ^{36}S events respectively, counted during the mass-36 measurement time t_{36}. $I_{^{35}\mathrm{Cl}}$ is the measured ^{35}Cl current, $e = 1.602 \times 10^{-19}$ C the elementary charge, and q the charge state number. The sulfur correction factor f_S was determined by counting ^{36}S from a stainless steel target and calculating the ratio of the ^{36}S events ending up in the ^{36}Cl region of interest to the ^{36}S events ending up in the sulfur region of interest. This isobar correction was typically well below 1% for irradiated samples and standards, except for the VERA beam time July-2009 where it was between 0.8% and 4%.

All data was normalized to the SM-Cl-11 standard. Data from beam times where other standards were used (see Table VIII) was re-normalized to the SM-Cl-11 standard using data from cross-calibration measurements [46]. The normalization factors for the measurements at DREAMS and HIAF were 11.39(5) and 1.00(2) respectively. Due to different beam energies and detector settings used in the five beam times at VERA, the normalization factors at VERA varied between 1.56 and 5.34 with typical uncertainties of ≈2%. In the next step a blank correction was applied, by subtracting the normalized ^{36}Cl/^{35}Cl ratio of the measured nonirradiated blank sample.

TABLE VIII. Calibration materials used for the normalization of the AMS results. Eventually all results were re-normalized to the standard material SM-Cl-11 [46].

Beam time	AMS facility	Calibration material	Nominal ^{36}Cl/^{35}Cl	Ref.
Mar-2009	VERA	ETH K381/4N	$2.262(8) \times 10^{-11}$	[58]
Jul-2009	VERA	DiluSe II	$1.63(11) \times 10^{-12}$	[59]
Nov-2009	VERA	ETH K381/4N	$2.262(8) \times 10^{-11}$	[58]
Feb-2010	VERA	ETH K381/4N	$2.262(8) \times 10^{-11}$	[58]
Apr-2010	VERA	ETH K381/4N	$2.262(8) \times 10^{-11}$	[58]
Sep-2014	DREAMS	SM-Cl-11	$1.424(13) \times 10^{-11}$	[46]
Mar-2015	HIAF	GEC	$4.43(3) \times 10^{-13}$	[60]
Oct-2015	HIAF	SM-Cl-11	$1.424(13) \times 10^{-11}$	[46]

A fractionation correction was required for the measurements at HIAF, by scaling the measured ^{36}Cl/^{35}Cl ratio with

$$f_f = 1 - 0.5\left[1 - \frac{\left(\frac{^{35}\mathrm{Cl}}{^{37}\mathrm{Cl}}\right)_n}{\left(\frac{^{35}\mathrm{Cl}}{^{37}\mathrm{Cl}}\right)_m}\right], \tag{A2}$$

where $\left(\frac{^{35}\mathrm{Cl}}{^{37}\mathrm{Cl}}\right)_n$ is the natural isotopic ratio of 3.125 and $\left(\frac{^{35}\mathrm{Cl}}{^{37}\mathrm{Cl}}\right)_m$ the measured isotopic ratio. These fractionation corrections were up to 2.7% at HIAF. For the measurements at DREAMS and VERA these differences were negligible. The most probable reason for the larger fractionation is the scaling of the terminal voltage between the three Cl isotopes, as pointed out in Sec. III B 3.

APPENDIX B: CONVOLUTION OF ENDF/B-VII.1 CROSS SECTION DATA WITH NEUTRON SPECTRA

Convolution of the ENDF/B-VII.1 cross section data with real Maxwell-Boltzmann neutron spectra and the modeled neutron spectra is done according to Eqs. (9) and (7) (see Sec. V in the main text), respectively. The modeled experimental neutron spectra are given in intervals of 1 keV. The energy cutoffs of the modeled data are at 114 and 200 keV for the PINO and SIMLIT simulations, respectively. In all cases, beyond these energies the relative neutron numbers per energy unit are in or below the 10^{-4} range of the interval with the maximum number of neutrons, hence they are negligible. The ENDF/B-VII.1 data and the simulated relative number of neutron per energy unit was interpolated in such a way that there are at least 900 data points (energy intervals) per decade. Hence, the maximum interval length is roughly 0.11% of the according energy decade, but can be significantly smaller in energy regions were resonances occur and the ENDF/B-VII.1 differential cross sections data points are denser.

[1] M. Busso, R. Gallino, and G. J. Wasserburg, Annu. Rev. Astron. Astrophys. **37**, 239 (1999).
[2] F. Käppeler, R. Gallino, S. Bisterzo, and W. Aoki, Rev. Mod. Phys. **83**, 157 (2011).
[3] P. Mohr, C. Heinz, M. Pignatari, I. Dillmann, A. Mengoni, and F. Käppeler, Astrophys. J. **827**, 29 (2016).
[4] M. Asplund, N. Grevesse, A. J. Sauval, and P. Scott, Annu. Rev. Astron. Astrophys. **47**, 481 (2009).

[5] H. Schatz, S. Jaag, G. Linker, R. Steininger, F. Käppeler, P. E. Koehler, S. M. Graff, and M. Wiescher, Phys. Rev. C **51**, 379 (1995).

[6] R. Reifarth, K. Schwarz, and F. Käppeler, Astrophys. J. **528**, 573 (2000).

[7] R. L. Macklin, Phys. Rev. C **29**, 1996 (1984).

[8] K. H. Guber, R. O. Sayer, T. E. Valentine, L. C. Leal, R. R. Spencer, J. A. Harvey, P. E. Koehler, and T. Rauscher, Phys. Rev. C **65**, 058801 (2002).

[9] W. Kutschera, Eur. Phys. J. Web Conf. **63**, 03001 (2013).

[10] H.-A. Synal, Int. J. Mass Spectrom. **349-350**, 192 (2013).

[11] A. Wallner, Nucl. Instrum. Methods Phys. Res., Sect. B **268**, 1277 (2010).

[12] N. Nica, J. Cameron, and B. Singh, Nucl. Data Sheets **113**, 1 (2012).

[13] H. Beer and R. L. Macklin, Phys. Rev. C **26**, 1404 (1982).

[14] S. E. Woosley, W. A. Fowler, J. A. Holmes, and B. A. Zimmerman, At. Data Nucl. Data Tables **22**, 371 (1978).

[15] T. Rauscher and F.-K. Thielemann, At. Data Nucl. Data Tables **75**, 1 (2000).

[16] S. Goriely, Hauser-Feshbach rates for neutron capture reactions, 2005, http://www-astro.ulb.ac.be, version 8/29/2005.

[17] M. Chadwick *et al.*, Nucl. Data Sheets **112**, 2887 (2011).

[18] OECD, JEFF-3.2 evaluated data library, OECD Nuclear Energy Agency technical report, 2014 (unpublishehed), http://www.oecd-nea.org/dbforms/data/eva/evatapes/jeff_32/

[19] K. Shibata, O. Iwamoto, T. Nakagawa, N. Iwamoto, A. Ichihara, S. Kunieda, S. Chiba, K. Furutaka, N. Otuka, T. Ohsawa, T. Murata, H. Matsunobu, A. Zukeran, S. Kamada, and S. Katakura, J. Nucl. Sci. Technol. **48**, 1 (2011).

[20] A. J. Koning and D. Rochman, Nucl. Data Sheets **113**, 2841 (2012).

[21] I. Dillmann, R. Plag, F. Käppeler, A. Mengoni, C. Heinz, and M. Pignatari, in Nuclei in the Cosmos XIII [PoS NIC XIII, 057 (2014)], http://pos.sissa.it

[22] W. Ratynski and F. Käppeler, Phys. Rev. C **37**, 595 (1988).

[23] S. Halfon, A. Arenshtam, D. Kijel, M. Paul, D. Berkovits, I. Eliyahu, G. Feinberg, M. Friedman, N. Hazenshprung, I. Mardor, A. Nagler, G. Shimel, M. Tessler, and I. Silverman, Rev. Sci. Instrum. **84**, 123507 (2013).

[24] S. Halfon *et al.*, Rev. Sci. Instrum. **85**, 056105 (2014).

[25] A. Kreisel *et al.*, in *Proceedings of Linac 2014*, edited by C. Carli, M. Draper, Y.-M. Ducimetiere, A. McCausey, R. Müller, J. Poole, V. R. W. Schaa (Geneva, Switzerland, 2014), p. 770.

[26] M. Martschini, P. Andersson, O. Forstner, R. Golser, D. Hanstorp, A. O. Lindahl, W. Kutschera, S. Pavetich, A. Priller, J. Rohlén, P. Steier, M. Suter, and A. Wallner, Nucl. Instrum. Methods Phys. Res., Sect. B **294**, 115 (2013).

[27] M. Martschini, O. Forstner, R. Golser, W. Kutschera, S. Pavetich, A. Priller, P. Steier, M. Suter, and A. Wallner, Nucl. Instrum. Methods Phys. Res., Sect. B **269**, 3188 (2011).

[28] G. Rugel, S. Pavetich, S. Akhmadaliev, S. M. Enamorado Baez, A. Scharf, R. Ziegenrücker, and S. Merchel, Nucl. Instrum. Methods Phys. Res., Sect. B **370**, 94 (2016).

[29] S. Pavetich, S. Akhmadaliev, M. Arnold, G. Aumaître, D. Bourlès, J. Buchriegler, R. Golser, K. Keddadouche, M. Martschini, S. Merchel, G. Rugel, and P. Steier, Nucl. Instrum. Methods Phys. Res., Sect. B **329**, 22 (2014).

[30] S. Akhmadaliev, R. Heller, D. Hanf, G. Rugel, and S. Merchel, Nucl. Instrum. Methods Phys. Res., Sect. B **294**, 5 (2013).

[31] L. K. Fifield, S. G. Tims, T. Fujioka, W. T. Hoo, and S. E. Everett, Nucl. Instrum. Methods Phys. Res., Sect. B **268**, 858 (2010).

[32] M. Berglund and M. E. Wieser, Pure Appl. Chem. **83**, 397 (2011).

[33] R. E. White, P. H. Barker, and D. M. J. Lovelock, Metrologia **21**, 193 (1985).

[34] H. Xiaolong, Nucl. Data Sheets **110**, 2533 (2009).

[35] R. Reifarth, M. Heil, F. Käppeler, and R. Plag, Nucl. Instrum. Methods Phys. Res., Sect. A **608**, 139 (2009).

[36] M. Friedman, D. Cohen, M. Paul, D. Berkovits, Y. Eisen, G. Feinberg, G. Giorginis, S. Halfon, A. Krása, A. J. M. Plompen, and A. Shor, Nucl. Instrum. Methods Phys. Res., Sect. A **698**, 117 (2013).

[37] G. Feinberg, Ph.D. thesis, Study of the ^{7}Li(p,n) Reaction Towards Measurements of Neutron-Capture Cross Sections in the Astrophysical s-process With the SARAF Accelerator and a Liquid-Lithium Target, Hebrew University of Jerusalem, 2014.

[38] G. Feinberg, M. Friedman, A. Krása, A. Shor, Y. Eisen, D. Berkovits, D. Cohen, G. Giorginis, T. Hirsh, M. Paul, A. J. M. Plompen, and E. Tsuk, Phys. Rev. C **85**, 055810 (2012).

[39] J. Allison *et al.*, IEEE Trans. Nucl. Sci. **53**, 270 (2006).

[40] S. Agostinelli *et al.*, Nucl. Instrum. Methods Phys. Res., Sect. A **506**, 250 (2003).

[41] J. O. Stone, G. L. Allan, L. K. Fifield, and R. G. Cresswell, Geochim. Cosmochim. Acta **60**, 679 (1996).

[42] N. J. Conard, D. Elmore, P. W. Kubik, H. W. Gove, L. E. Tubbs, B. A. Chrunyk, and M. Wahlen, Radiocarbon **28**, 556 (1986).

[43] W. Kutschera, P. Collon, H. Friedmann, R. Golser, P. Hille, A. Priller, W. Rom, P. Steier, S. Tagesen, A. Wallner, E. Wild, and G. Winkler, Nucl. Instrum. Methods Phys. Res., Sect. B **123**, 47 (1997).

[44] P. Steier, R. Golser, W. Kutschera, A. Priller, C. Vockenhuber, and S. Winkler, Nucl. Instrum. Methods Phys. Res., Sect. B **223-224**, 67 (2004).

[45] A. Priller, M. Auer, R. Golser, A. Herschmann, W. Kutschera, J. Lukas, P. Steier, and A. Wallner, Nucl. Instrum. Methods Phys. Res., Sect. B **259**, 94 (2007).

[46] S. Merchel *et al.*, Anal. Bioanal. Chem. **400**, 3125 (2011).

[47] O. Forstner, L. Michlmayr, M. Auer, R. Golser, W. Kutschera, A. Priller, P. Steier, and A. Wallner, Nucl. Instrum. Methods Phys. Res., Sect. B **266**, 2213 (2008).

[48] S. Pavetich, Ph.D. thesis, Determination of non-routine radionuclides by medium-energy accelerator mass spectrometry, Technische Universität Dresden, Fakultät für Physik, 2015.

[49] L. K. Fifield, S. G. Tims, J. O. Stone, D. C. Argento, and M. De Cesare, Nucl. Instrum. Methods Phys. Res., Sect. B **294**, 126 (2013).

[50] I. Dillmann, C. Domingo-Pardo, M. Heil, F. Käppeler, A. Wallner, O. Forstner, R. Golser, W. Kutschera, A. Priller, P. Steier, A. Mengoni, R. Gallino, M. Paul, and C. Vockenhuber, Phys. Rev. C **79**, 065805 (2009).

[51] A. Wallner, K. Buczak, T. Belgya, M. Bichler, L. Coquard, I. Dillmann, R. Golser, F. Käppeler, A. Karakas, W. Kutschera, C. Lederer, A. Mengoni, M. Pignatari, A. Priller, R. Reifarth, P. Steier, and L. Szentmiklosi, Phys. Rev. C **96**, 025808 (2017).

[52] A. Wallner, T. Belgya, M. Bichler, K. Buczak, I. Dillmann, F. Käppeler, C. Lederer, A. Mengoni, F. Quinto, P. Steier, and L. Szentmiklosi, Phys. Rev. Lett. **112**, 192501 (2014).

[53] A. Wallner, M. Bichler, K. Buczak, I. Dillmann, F. Käppeler, A. Karakas, C. Lederer, M. Lugaro, K. Mair, A. Mengoni, G. Schätzel, P. Steier, and H. P. Trautvetter, Phys. Rev. C **93**, 045803 (2016).

[54] S. Jaag, J. Ostermöller, R. Plag, R. Reifarth, S. Schmidt, and M. Weigand, NETZ: Simulating s-Process Nucleosynthesis, Goethe University Frankfurt technical report, 2013 (unpublished), http://exp-astro.physik.uni-frankfurt.de/netz/

[55] M. Weigand *et al.*, Phys. Rev. C **92**, 045810 (2015).

[56] Z. Y. Bao, H. Beer, F. Käppeler, F. Voss, K. Wisshak, and T. Rauscher, At. Data Nucl. Data Tables **76**, 70 (2000).

[57] S. Merchel, R. Braucher, V. Alfimov, M. Bichler, D. L. Bourlès, and J. M. Reitner, Quaternary Geochronology **18**, 54 (2013).

[58] V. Alfimov, H. Synal, R. Finkel, and K. Wilcken, Re-calibration of ETH Chlorine-36 Standards, Ion Beam Physics, ETH Zürich annual report, 2009.

[59] M. Martschini, Ph.D. thesis, Development of methods for isobar suppression in AMS and measurements of ^{36}Cl with the VERA 3-MV-tandem accelerator, Universität Wien, Fakultät für Physik, 2012.

[60] L. K. Fifield, T. R. Ophel, G. L. Allan, J. R. Bird, and R. F. Davie, Nucl. Instrum. Methods Phys. Res., Sect. B **52**, 233 (1990).